Results in Engineering 25 (2025) 104029

Contents lists available at ScienceDirect

Results in Engineering

journal homepage: www.sciencedirect.com/journal/results-in-engineering

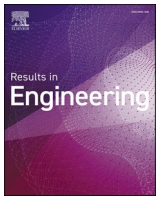

Finite element analysis and experimental verification of press-fit peg push-in and pull-out in trabecular bone analogue

Xiaoyi Min *, David Heath, Azmi Rahman, Laurence Marks, David Murray, Stephen Mellon

Nuffield Department of Orthopaedics, Rheumatology and Musculoskeletal Sciences, University of Oxford, Oxford, United Kingdom

ARTICLE INFO

Keywords:
Finite element modelling
Primary fixation
Press-fit
Explicit FEA
Cementless implants

ABSTRACT

Aims: Primary fixation of cementless implants is achieved through press-fit. This study aimed to simulate the press-fit of pegs in bone analogue with finite element analysis (FEA) with as few parameters as possible, thereby providing a useful tool for the quick evaluation of potential device designs.
Methods: Push-in and pull-out of smooth and porous pegs in plastic trabecular bone analogue (20 PCF, Sawbones) were modelled using a finite element approach. The model was validated by comparing the maximum push-in and pull-out forces from FEA to the corresponding peg push-in/pull-out testing in plastic bone.
Results: The results from FEA agreed well with experiments for the smooth pegs at surgically-relevant interferences (0.6–0.9 mm). Error was under 18.4 % for maximum push-in forces and 6.9 % for maximum pull-out forces. When the same fracture strain value was used to simulate porous pegs, the errors were 9.4 % and 14.7 % for push-in and pull-out force, respectively.
Conclusion: The proposed method of simulating peg press-fit required only two sets of input data: the uniaxial material curve of the plastic bone from which the fracture strain could also be derived, and the coefficient of friction between the plastic bone and the peg. The method can be applied to gain insight into the potential of new fixation component designs before progression to experimental testing.

1. Introduction

The cemented total knee replacement (TKR) had been the gold standard treatment for knee osteoarthritis until the 1980s when interest in cementless fixation started to grow [1]. Cementless fixation was introduced to avoid complications related to the failure of cement or cementation errors [2]. However, the popularity of cementless implants declined as poor early results and high rates of loosening were seen due to inadequate osseointegration at the bone-implant contact interface [3]. Until now, cemented TKR remains the most commonly performed primary knee procedure in the UK with excellent long-term outcomes, making up 83 % of all types of primary knee replacements in 2022 [4]. The use of cementless TKRs dropped from 3.6 % of all total knee replacement procedures to 2.5 % in the UK from 2012 to 2022 due to concerns that arose from the high early failure rate [4,5]. However, the proportion of cementless TKRs implanted in the US has increased from 1.9 % to 20.5 % from 2012 to 2022 due to the advantages of shorter operation time and potential improvement in long-term fixation [6,7]. Though cementless TKR became less popular in the UK, there was a significant increase in the use of cementless/hybrid unicompartmental knee replacement (UKR) in the past decade, with the proportion increasing from 14.8 % of all UKRs in 2012 to 36.8 % in 2022 [4].

Current designs of cementless knee implants have porous surfaces on the fixation elements, which facilitate bone ingrowth, and usually have hydroxyapatite (HA) coatings, intended to improve osseointegration at the contact interface [8]. Improved component designs and materials have revived interest in cementless fixation which offers several potential benefits: better preservation of bone stock, reduced rate of complications due to cement failure, and better long-term fixation through osseointegration [9,10]. Excellent long-term clinical and radiographic results of the cementless UKR have also been reported, with a 10-year survival of 97 % [11].

Primary fixation of cementless implants comes from the stress induced in the periprosthetic bone when the component is press-fit into an undersized cavity with compression [8]. This periprosthetic stress and subsequent frictional force at the bone-implant contact interface hold the component in place [12], and inhibit excessive micromotion which leads to the formation of fibrous tissue in place of bone at the

* Corresponding author.
E-mail addresses: xiaoyi.min@ndorms.ox.ac.uk (X. Min), david.heath@ndorms.ox.ac.uk (D. Heath), azmi.rahman@ndorms.ox.ac.uk (A. Rahman), laurence.marks@ndorms.ox.ac.uk (L. Marks), david.murray@ndorms.ox.ac.uk (D. Murray), stephen.mellon@ndorms.ox.ac.uk (S. Mellon).

https://doi.org/10.1016/j.rineng.2025.104029
Received 13 August 2024; Received in revised form 20 December 2024; Accepted 13 January 2025
Available online 14 January 2025
2590-1230/© 2025 The Authors. Published by Elsevier B.V. This is an open access article under the CC BY license (http://creativecommons.org/licenses/by/4.0/).

contact interface and negatively affects implant fixation [13,14]. Successful primary fixation appears to be a prerequisite for a satisfactory secondary fixation which is achieved through bone ingrowth and osseointegration at the bone-implant interface during bone healing [15,16]. The maximum force required to push in the cementless component is commonly used as a measure of the risk of periprosthetic fracture with excessive stresses induced during implantation being a risk factor [17,18]. A higher push-in force implies more deformation and larger stress and strain induced in bone, which as a result weakens its load-bearing ability [17,19]. The maximum force required to pull out the component is often used as a measure to assess primary fixation [18,20]. To pull-out a component, the load applied needs to overcome the friction force at the bone-implant contact interface and counteract the gripping force on the component generated by the interference fit. If the component is not adequately fixed, these forces holding the component in place might not be able to resist its movement relative to the interfacing bone under loading during the bone healing stage. This low pull-out force implies a lower force threshold that needs to be overcome to induce implant micromotion, which can negatively affect fixation [18].

When simulating the physical process of implant insertion, an implicit solver faces convergence problems due to nonlinearity in contact and material properties from extreme deformation in the host bone. Hence, previous attempts at modelling press-fit implantation with finite element analysis (FEA) generally involved an interference fit contact with the resolution of an initial overclosure using an implicit solver [21,22]. The implant penetrates the bone at the start of the analysis and an interference fit contact algorithm is applied which pushes the bone elements outwards until there is no more penetration. Bone was generally modelled as a linear elastic or linear elastic-plastic material with material properties assigned based on the bone density converted from the CT scans of the implantation sites, which were subject-specific [21,22]. This method has a number of disadvantages and limitations. Firstly, it cannot make an estimate of the push-in force as this part of the physical process is not modelled. Secondly, it cannot consider the process by which material is actually removed at the bone-implant interface by extreme deformations and machining/abrading during implant insertion. For this reason, it was decided that an explicit solver with element deletion could be used to provide a means of estimating these effects without significant overhead, and critically without this causing the solution to terminate.

Bone, with a complicated cellular microstructure, shows asymmetric compressive and tensile behaviours [23]. The properties also vary greatly among individuals and among resection sites [24]. This again creates large complexity when developing computational models of implant press-fit for the assessment of primary fixation. Analogues of trabecular bone, 20 pounds per cubic foot (PCF) (0.32 g/cm^3) polyurethane foam as an example, are frequently used for benchtop experiments to obtain insights into the effects of design and surgical factors on primary fixation [18,25–27]. It exhibits much less variability compared to real bone. Moreover, the use of polyurethane foam is more accessible and controllable for benchtop experimental validations of the computational models. Thus, we have modelled the press-fit behaviour of pegs in polyurethane foam rather than trabecular bone.

The objective of this study was to develop a simple FEA model that could quickly computationally simulate the physical process of cementless component press-fit for the assessment of primary fixation. The model should be able to predict the maximum push-in and pull-out forces of cementless implants in the trabecular bone analogue with good accuracy, requiring minimal parameter inputs. The method was validated by comparing the results from the model to the corresponding experiment conducted in plastic bone.

2. Methods

2.1. Finite element simulations

An FE model was built in Abaqus CAE with the Explicit solver (Abaqus 2020, Dassault Systèmes) to simulate the push-in/pull-out (PIPO) of pegs, which are a widely used fixation element in orthopaedics.

Three straight titanium pegs of 5.7 mm diameter (smooth surface) and 4.7 mm diameter (1 with smooth surface and 1 with porous surface) with a circular cross-section and a hemispherical tip were modelled. A homogeneous plastic bone analogue (Sawbones Solid Rigid Polyurethane Foam, PCF20, #1522–03, Malmö, Sweden) with relatively predictable material properties was modelled in this study. It is seen as an analogue for trabecular bone and the chosen density is most commonly used for biomechanical testing [18,25–28].

2.1.1. Model geometry and boundary conditions

An axisymmetric model was built to save computational costs. A cylindrical plastic bone of 22.45 mm in diameter and 35.00 mm in height was modelled. Holes of different diameters were modelled to simulate press-fit at surgically-relevant diametral interferences of 0.68, 0.70 and 0.92 mm with the 5.7 mm smooth peg [18,29]. A smaller interference of 0.45 mm and a larger interference of 1.06 mm were also tested. Interference of 0.60 mm was tested with the 4.7 mm smooth peg and porous peg. 4.7 mm is the mean diameter of the porous peg which was the centre line of the asperities. The diameters of the 3D-printed porous peg simulated in the model were measured with a vernier calliper (500–196–20, Mitutoyo, Kawasaki, Japan). The maximum diameter of the porous peg that took the height of the asperities on the porous surface into account was 4.8 mm. To model the PIPO of the porous peg considering the effect of the asperities on the rough surface, a 4.8 mm porous peg was also tested at the interference of 0.70 mm. All holes were 15 mm in depth. An explicit solver was chosen to avoid convergence issues caused by the excess distortion of elements during peg insertion. The foam was constrained in the vertical direction at the bottom edge and was fixed in the radial direction on the side which represents the constraining effects from the rest of the bone block around the tested hole. All other edges were free to move. The peg was pushed 9.0 mm into the hole and was pulled out completely through a vertical displacement applied to a reference point assigned to the top of the peg. All other degrees of freedom of the peg were constrained to avoid rigid body motion (Fig. 1).

2.1.2. Material

The material properties of the titanium peg and the plastic bone are listed in Table 1. The Young's modulus of the plastic bone was obtained from a uniaxial compression test on the Sawbones foam.

As the metal peg was several orders of magnitude stiffer than the foam, it was modelled as rigid. The foam was modelled as a deformable material the plasticity of which was applied using the material curve derived from the uniaxial compression test results (Fig. 2).

Press-fit insertion at interferences above a certain level causes both extreme deformation and material removal at the bone-implant interface [30,31]. This is problematic with implicit finite element modelling as it causes large element distortion and lack of convergence. The ductile damage feature in Abaqus/Explicit was used to implement element deletion which could overcome the convergence issue that occurred with implicit solver, and go some way towards modelling the combined effect of extreme deformation and machining in foam. The deletion of elements was defined by the fracture strain input which was the threshold strain value above which the element would be removed. The fracture strain was tuned using data from PIPO experiments of the 5.7 mm smooth peg. Fracture strain values of 0.31, 0.28 and 0.34 (±10 % of the upturn value on the true stress-true strain curve, 0.31), were tested with the 5.7 mm smooth peg. The maximum push-in forces and the

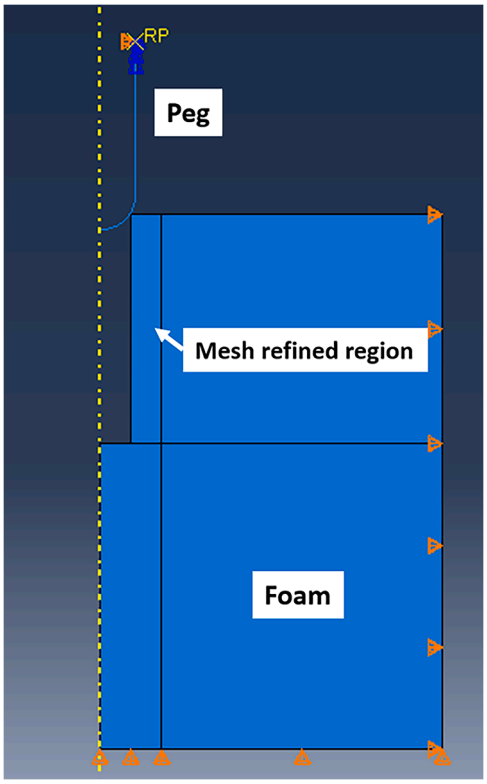

Fig. 1. Axisymmetric finite element model setup.

Table 1
Material properties of 3-D printed pegs and Sawbones foam.

	Young's modulus (MPa)	Poisson ratio
Titanium Peg	Rigid body	Rigid body
Plastic bone	160	0.3

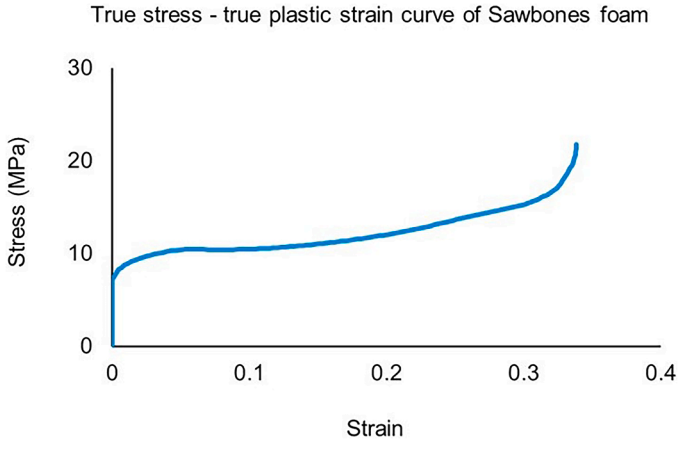

Fig. 2. True stress-true plastic strain curve of the Sawbones foam. The upturn value is 0.31 at which the gradient of the curve greatly increases.

maximum pull-out forces required in the simulations at each fracture strain were compared to those from the experiments. The fracture strain value that gave results closest to the experiments was then applied to simulate the PIPO of 4.7 mm smooth and porous pegs at an interference of 0.60 mm and the PIPO of the 4.8 mm porous peg at an interference of 0.70mm.

2.1.3. Mesh

The side wall of the peg was meshed with elements of 0.5 mm and the peg tip was meshed with elements of 0.2 mm to capture the shape of the curvature. The plastic bone was meshed with CAX4R axisymmetric elements. Mesh was refined in the region 2 mm radial from the hole surface to improve solution efficiency. Mesh convergence studies were conducted for the 5.7 mm smooth peg at each interference. The criterion was that the change in maximum push-in force and maximum pull-out force should be within 5 % of those from the previous simulation while the mesh size was gradually decreased. The mesh sizes used for the interference of 0.68, 0.70, 0.92 and 1.06 mm were 0.05, 0.05, 0.06 and 0.05 mm respectively. For interference of 0.45 mm, the pull-out force failed to converge when the mesh size was reduced from 0.06 to 0.03 mm. As the model of 0.03 mm required excessive analysis time, elements of 0.04 mm were used.

For the simulations of the 4.7 mm smooth peg, the mesh in the refined region was set to 0.03 mm from which the maximum push-in and pull-out forces started to converge. The same mesh size was used for the porous peg.

2.1.4. Contact

The contact between the peg and the foam was modelled using the Coulomb friction model with coefficients of friction found from an experimental friction study [32]. The difference in surface roughness between the smooth and porous peg was modelled by applying the respective coefficient of friction found in the experiment (smooth: 0.27; porous: 0.56). An eroding surface contact was defined. As the elements near the hole were deleted during insertion, the contact interface was constantly renewed and updated so that a frictional relationship was set up between the new foam surface and the peg.

Insertion of the porous peg was modelled twice using the mean diameter (4.70 mm) and the maximum diameter (4.80 mm) of the peg respectively. The maximum diameter took the surface height of the asperities on the peg surface into account. The same coefficient of friction was used in both simulations.

2.2. Experimental validations

A benchtop PIPO experiment was conducted to examine the accuracy and reliability of the FE model (Fig. 3). Straight 3D-printed titanium pegs (Cp-Ti Grade 2, AP&C, Saint-Eustache, Canada) with a circular cross-section and a hemispherical tip were pushed in and pulled out from pre-drilled holes in a Sawbones plastic bone block using the DARTEC HC-10 servohydraulic material testing machine (ZwickRoell Ltd, Herefordshire, UK) and FSB-01 S-beam load cell (Force Logic, Berkshire, UK). Three peg designs were tested: 5.7 mm diameter smooth peg, 4.7 mm diameter smooth peg and 4.7 mm diameter porous peg, as in the FE models (Fig. 4).

Holes of different sizes were prepared using a pillar drill in the plastic bone to achieve the interferences tested in the FE models. All holes were 15 mm deep. The test was repeated 3 times at each interference with the 5.7 mm peg and was repeated 6 times with the 4.7 mm pegs at 0.6 mm interference.

The peg was aligned to the hole manually before each test. It was then pushed in by 9.0 mm at 10 mm/min and completely pulled out at the same rate under displacement control. The plastic bone block was constrained in the anterior-posterior direction. The forces applied by the load cell were recorded at a frequency of 250 Hz.

3. Results

The maximum forces required to push in and pull out the 5.7 mm smooth peg from the FE model were compared to those recorded from the experiment. When the fracture strain value was set to $\varepsilon_p = 0.31$, the results from the simulations for 0.68, 0.70 and 0.92 mm interferences, which were the surgically-relevant interferences, agreed well with the

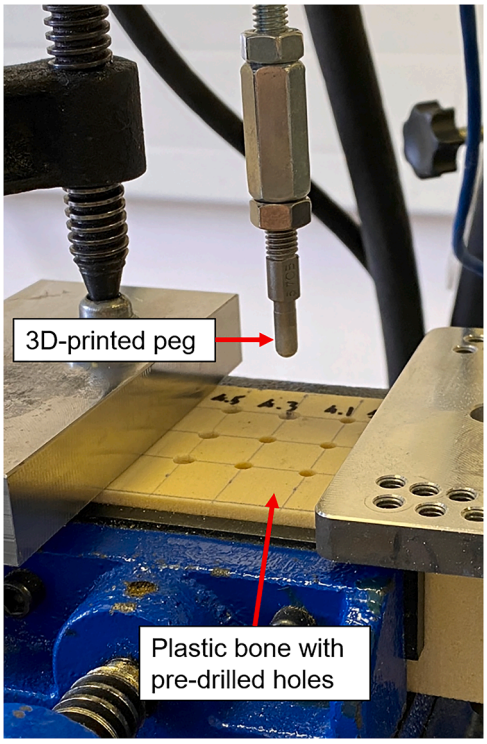

Fig. 3. Experimental setup.

Fig. 4. Pegs of smooth (left) and porous (right) surface finish.

experiment. The force-displacement curves from the model showed a similar shape and trend to the experimental curves (Fig. 5). Maximum pull-out forces at all three interferences were within ±7 % of the experiment results. Errors of the maximum push-in forces were +18.4 %, +10.2 % and −1.5 % at 0.68, 0.70 and 0.92 mm interference respectively, all within ±20 % from the experimental mean. The same fracture strain, however, gave larger errors at a smaller interference of 0.45 mm (+46.4 % for maximum push-in force; +21.4 % for maximum pull-out force) and a larger interference of 1.06 mm (−14.4 % for maximum push-in force; −22.9 % for maximum pull-out force) (Table 2).

Using the same fracture strain value of 0.31, the simulation of the smooth peg of 4.7 mm diameter gave a force-displacement curve in good accordance with the experimental curves (Fig. 6). Both the maximum push-in force and maximum pull-out force were within ±14 % of the experimental results (Table 3).

For the simulation of the 4.7 mm porous peg, similar to what was found in the experiment, the porous coating reduced both the push-in force and the pull-out force compared to the smooth one when either the mean diameter or the maximum diameter was used (Fig. 7). The porous peg also gave smaller pull-out force/push-in force ratios compared to the smooth peg as observed in the experiment when either dimension was used. When the mean diameter was used, the percentage error was +13.7 % for the push-in force while the pull-out force was overestimated by 32 % (Table 3). A deviation in the shape of the curve was shown in the force-displacement graph (Fig. 8). When the maximum diameter of the porous peg was used, the percentage error was +9.4 % for the push-in force and +14.7 % for the pull-out force. Simulation using the maximum diameter of the peg gave both maximum push-in force and maximum pull-out force closer to the experiment results compared to when using the mean diameter.

4. Discussion

Finite element simulations of cementless component implantation have great complexity as 1) bone has a complicated cellular micro-structure, shows non-linear and asymmetric behaviours under compression and tension [23], and is subject-specific, and 2) it is computationally difficult to simulate the physical process of press-fit due to nonlinearity from the large deformation in the periprosthetic bone at high interference.

Bone damage is inevitable at anything other than very light interference, combining extreme material deformation, abrasion and machining [30]. In this study, an explicit solver was chosen to overcome the convergence issue that appears with an implicit solver when dealing with nonlinearity from large material deformation. The technique of element deletion was used to model the combined bone damage effect rather than attempting to capture individual responses under press-fit. Trabecular bone analogue (20 PCF polyurethane foam), a homogeneous material that exhibits low variability in material properties [28, 33] compared to real bone was used in this study to minimise the impact of complicated material definitions. The polyurethane foam goes through three phases under compression: elastic stage, plateau stage, and densification stage [34]. In the plateau phase which is the part of the curve with small gradients in Fig. 2, the material goes through plastic deformation and the cellular structure collapses. Once the cells in the cellular foam cannot collapse further (e.g. when the upturn plastic strain value of the curve in Fig. 2, 0.31 is reached), the material starts to go through densification. The stress increases rapidly with little increase in strain. This behaviour was typically captured with damage models that required complex material definitions or with micro-FE models built from micro-CT scans, denoting the microstructure of the material [35, 36]. This study focuses on simplifying the computational simulations of complex material responses during press-fit with a single modelling technique.

The current study demonstrated that simulating the press-fit of a metal peg into polyurethane foam while using a strain threshold for the deletion ('fracture') of foam elements can accurately reproduce push-in and pull-out loads from experimental tests and provide an insight into the primary stability of press-fit fixation components.

The results from FEA agreed well with experiments for the smooth pegs at surgically-relevant interferences (0.6–0.9 mm) when the fracture strain was set to 0.31, which correlates to the upturn value on the true stress-true plastic strain curve of the Sawbones foam. Error was under 18.4 % for maximum push-in forces and 6.9 % for maximum pull-out forces. The progression of push-in and pull-out forces with

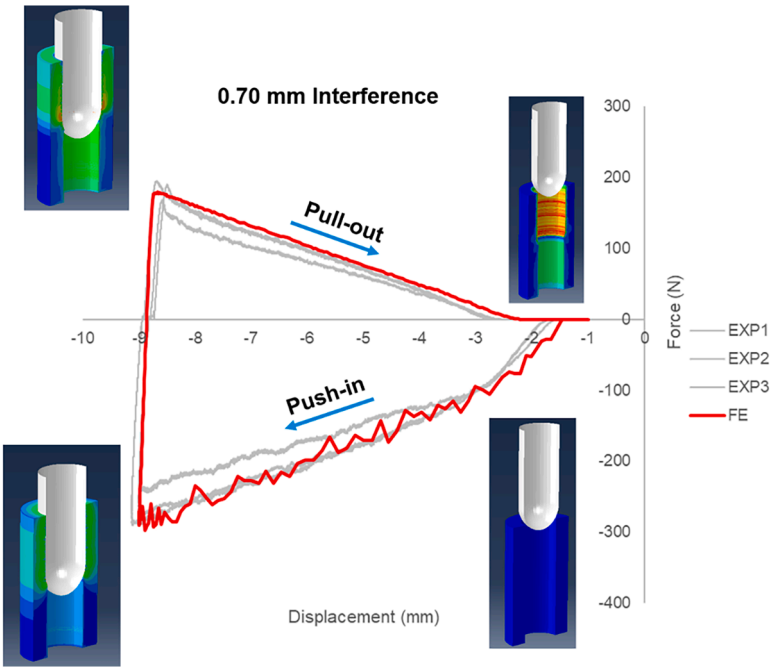

Fig. 5. Force-displacement curve from experiments (grey) and from FEA (red) of the PIPO of the smooth 5.7 mm peg at 0.70 mm interference with the fracture strain of 0.31.

Table 2
Maximum push-in and pull-out forces from experiment and FE model of the 5.7 mm smooth peg with fracture strain (FS) of 0.28, 0.31 and 0.34. FS of 0.31 gave results closest to experiments.

Interference (mm)		Push-in (N)	% error	Pull-out (N)	% error
0.45	**Experiment**	178.4 (SD = 4.9)	–	148.5 (SD=6.1)	–
	FS = 0.31	261.1	+46.4 %	180.3	+21.4 %
0.68	**Experiment**	244.5 (SD = 8.0)	–	179.5 (SD = 4.7)	–
	FS = 0.28	283.0	+15.7 %	175.1	−2.5 %
	FS = 0.31	289.6	+18.4 %	172.8	−3.7 %
	FS = 0.34	357.4	+46.2 %	204.4	+13.9 %
0.70	**Experiment**	270.2 (SD = 23.8)	–	184.6 (SD = 14.1)	–
	FS = 0.28	291.1	+7.7 %	180.1	−2.4 %
	FS = 0.31	297.8	+10.2 %	179.2	−2.9 %
	FS = 0.34	362.3	+34.1 %	219.0	+18.6 %
0.92	**Experiment**	349.4 (SD = 15.3)	–	206.9 (SD = 9.7)	–
	FS = 0.28	274.5	−21.4 %	135.1	−34.7 %
	FS = 0.31	344.0	−1.5 %	192.7	−6.9 %
	FS = 0.34	357.8	+2.4 %	174.9	−15.5 %
1.06	**Experiment**	373.9 (SD = 18.1)	–	201.1 (SD = 7.5)	–
	FS = 0.31	320.2	−14.4 %	155.0	−22.9 %

displacement also showed a similar trend to the experiment. Furthermore, when the same fracture strain value was used to simulate porous pegs PIPO, a reduction in maximum push-in force, maximum pull-out force and pull-out force/pull-in force ratio compared to the 4.7 mm smooth peg was shown, similar to what was observed in the experiment. The simulation gave results closer to the experimental results when the maximum diameter of the porous peg which considered the height of the asperities was used instead of the mean diameter. As the press-fit of pegs machines away the material around the hole, the peak height of asperities determines the amount of material that will be removed.

To the best of the authors' knowledge, this is the first study that computationally simulates the press-fit of both smooth and porous implants in bone analogue. Good accuracy was achieved in the prediction of maximum push-in force, maximum pull-out force and force-displacement curve shape within a reasonable simulation run time. The simulations were run on Microsoft Windows (Intel® Core™ i7–10,700 CPU @ 2.90 GHz, 32 GB RAM) for 3 to 10 h per sample depending on mesh size. The method can be applied to computationally test new fixation component designs efficiently before in vitro testing.

While the model in this study provided results that agreed well with experiments, some limitations require further investigation. The model gave less accurate results at 0.45 and 1.06 mm interferences which were outside the medium range (0.6–0.9 mm), and it was also hard to achieve mesh convergence at low interference. This could be attributed to the difference in damage mechanism at different levels of interference. At lower interferences, the deformation might be more dominated by elasticity and plasticity while at higher interferences, the deformation might be more damage-dominated [30]. As the fracture strain threshold in this element deletion technique aims to represent the combined material response after press-fit, the value may need to be adjusted accordingly when simulating interferences outside the surgically-relevant range of interest to this study. Secondly, this model does not distinguish between compressive and tensile deformation of plastic bone and assumes that the foam acted as an isotropic material. Characterisation of the tensile and anisotropic properties of bone in future models will further improve the accuracy when simulating the press-fit of implants in real bone. Thirdly, the shape of the force-displacement curves of the porous peg depends on the asperity morphology along the length of the peg. Thus, it was hard to achieve the same curve shape with a simple model that controlled surface contact with a single friction coefficient. Despite the slight differences in force-displacement curve shape, when the maximum diameter that represents the maximum asperity height was used, the similarity in FEA

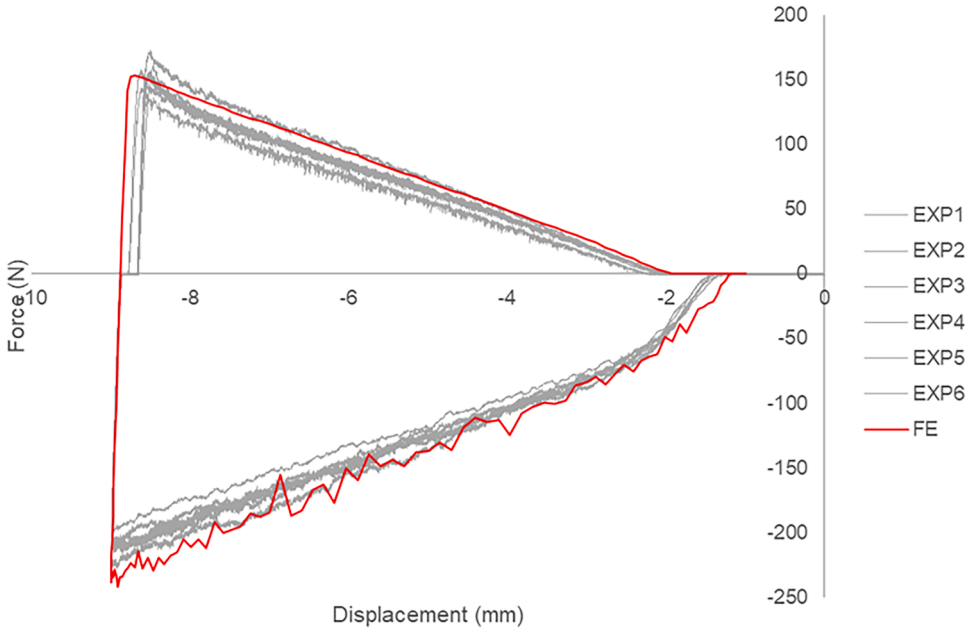

Fig. 6. Force-displacement curve at 0.6 mm interference for the smooth 4.7 mm peg.

Table 3
Maximum push-in and pull-out forces for the 4.7 mm smooth and 4.7 mm porous peg from experiments and FE model.

	Experiment push-in (N)	FE push-in (N)	% error	Experiment pull-out (N)	FE pull-out (N)	% error
4.7 mm smooth	212.7 (SD = 9.3)	241.2	+13.4 %	157.8 (SD = 9.6)	153.4	−2.8 %
4.7 mm porous	198.0 (SD = 3.8)	225.1	+13.7 %	88.6 (SD = 6.6)	117.0	+32.1 %
4.8 mm porous	198.0 (SD = 3.8)	216.6	+9.4 %	88.6 (SD = 6.6)	101.6	+14.7 %

and experimental maximum push-in force, maximum pull-out force and pull-out force/push-in force ratio implied that this simple model could be used to assess and compare primary fixation of different porous component designs within a reasonable time frame. Lastly, the element deletion technique produces oscillations on the push-in curve. As the component was pushed-in, deletion of an element would create a slight reduction in the push-in force required until the implant came into contact with the neighbour elements of that deleted, bringing oscillations to push-in section of the force-displacement curve. These oscillations were also presented in a previous FE study [35] and in the experimental results where push-in forces gave rough curves while the pull-out curves were much smoother. These oscillation could be reduced by increasing the number of elements. However, this would greatly increase the computational efforts without significantly changing the

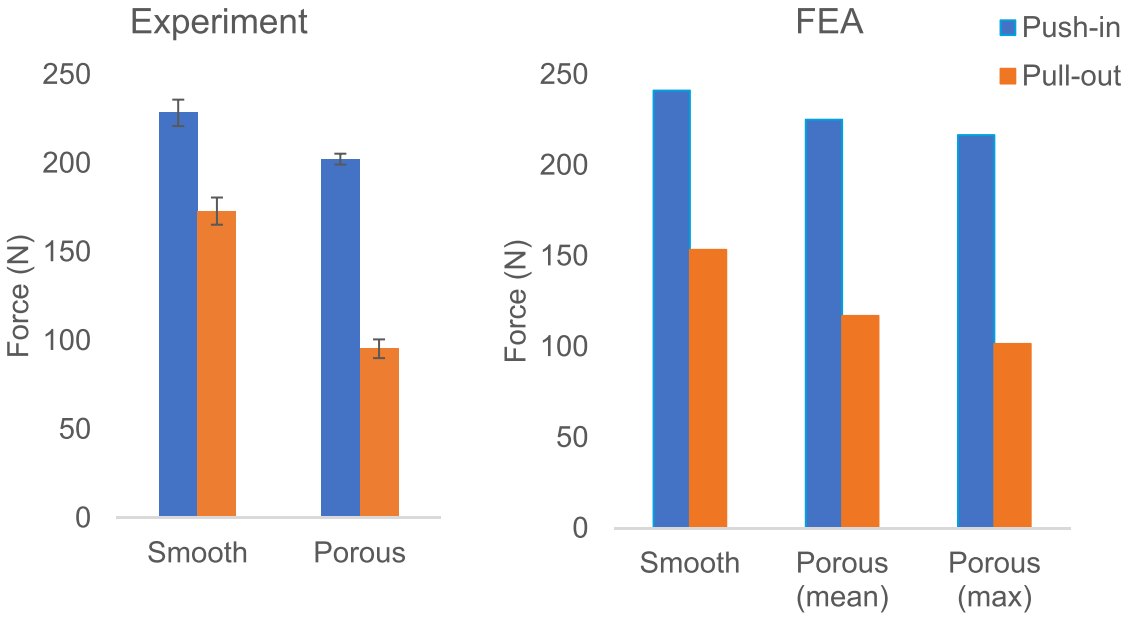

Fig. 7. Push-in and pull-out forces from the experiment with a 95 % confidence interval (left) and FE model (right) of the smooth and porous pegs of 4.7 mm diameter. The porous peg was modelled with mean diameter (4.7 mm) and maximum diameter (4.8 mm).

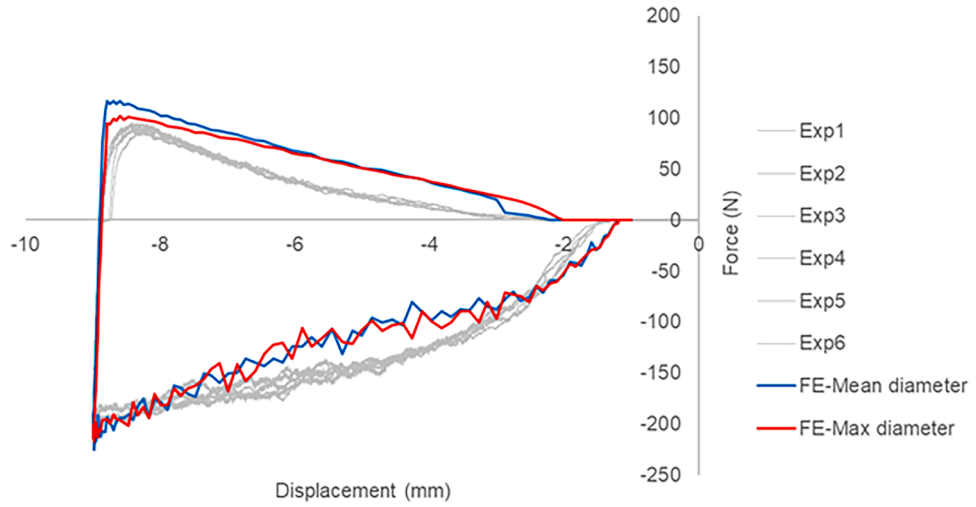

Fig. 8. Force-displacement curve for the porous 4.7 mm peg. FE simulation was conducted with both the mean diameter (0.60 mm interference) and the maximum diameter (0.70 mm interference) of the peg.

conclusion.

5. Conclusion

The explicit FE model of peg press-fit in plastic bone analogue required only two sets of inputs: the uniaxial material curve of the plastic bone from which the fracture strain value could also be found, and the coefficient of friction between the plastic bone and the implant. The results from the FE models showed good accordance with experimental results. The model can be applied to quickly computationally simulate the physical process of press-fit.

Funding

None

Ethical approval

Not required

CRediT authorship contribution statement

Xiaoyi Min: Writing – original draft, Software, Methodology, Investigation, Formal analysis. **David Heath:** Writing – review & editing, Methodology, Investigation. **Azmi Rahman:** Writing – review & editing, Methodology, Investigation. **Laurence Marks:** Writing – review & editing, Supervision, Project administration, Methodology. **David Murray:** Writing – review & editing, Supervision, Project administration, Methodology. **Stephen Mellon:** Writing – review & editing, Supervision, Project administration, Methodology.

Declaration of competing interest

The author or one or more of the authors have received or will receive benefits for personal or professional use from a commercial party related directly or indirectly to the subject of this article. In addition, benefits have been or will be directed to a research fund, foundation, educational institution, or other non- profit organisation with which one or more of the authors are associated.

Data availability

No data was used for the research described in the article.

References

[1] P.F. Helvie, E.R. Deckard, R.M. Meneghini, Cementless total knee arthroplasty over the past decade: excellent survivorship in contemporary designs, J. Arthroplasty. 38 (6S) (2023) S145–SS50.
[2] H.R. Mohammad, G.S. Bullock, J.A. Kennedy, et al., Cementless unicompartmental knee replacement achieves better ten-year clinical outcomes than cemented: a systematic review, Knee Surg. Sports Traumatol. Arthrosc. 29 (10) (2021) 3229–3245.
[3] F. Matassi, C. Carulli, R. Civinini, et al., Cemented versus cementless fixation in total knee arthroplasty, Joints. 1 (3) (2013) 121–125.
[4] National Joint Registry, NJR 20th Annual Report 2023, National Joint Registry, 2023.
[5] H.R. Mohammad, A. Judge, D.W. Murray, A matched comparison of the long-term outcomes of cemented and cementless total knee replacements: an analysis from the National Joint Registry of England, Wales, Northern Ireland and the Isle of Man, J. Bone Joint Surg. Am. 103 (24) (2021) 2270–2280.
[6] S. Puri, K. Alpaugh, Y.-F. Chiu, et al., Cementless versus cemented total knee arthroplasty of the same design: shorter operative times and minimal differences in early outcomes, HSS. J. (2023).
[7] American Joint Replacement Registry 2023 Annual Report, American Academy of Orthopaedic Surgeons, 2023.
[8] Q.M. Nguyen, Y. Otsuka, Y. Miyashita, Finite element simulations on delamination-induced local stress shielding effects on aseptic loosening behavior by bone remodeling, Results. Eng. 23 (2024).
[9] A.K. Prasad, J.H.S. Tan, H.S. Bedair, et al., Cemented vs. cementless fixation in primary total knee arthroplasty: a systematic review and meta-analysis, EFORT. Open. Rev. 5 (11) (2020) 793–798.
[10] A. Asokan, R. Plastow, B. Kayani, et al., Cementless knee arthroplasty: a review of recent performance, Bone Jt. Open. 2 (1) (2021) 48–57.
[11] H.R. Mohammad, J.A. Kennedy, S.J. Mellon, et al., Ten-year clinical and radiographic results of 1000 cementless Oxford unicompartmental knee replacements, Knee Surg. Sports Traumatol. Arthrosc. 28 (5) (2020) 1479–1487.
[12] D. O'Sullivan, L. Sennerby, D. Jagger, et al., A comparison of two methods of enhancing implant primary stability, Clin. ImPlant Dent. Relat. Res. 6 (1) (2004) 48–57.
[13] E. De Vries, E. Sanchez, D. Janssen, et al., Predicting friction at the bone - Implant interface in cementless total knee arthroplasty, J. Mech. Behav. Biomed. Mater. 128 (2022) 105103.
[14] N. Kohli, J.C. Stoddart, R.J. van Arkel, The limit of tolerable micromotion for implant osseointegration: a systematic review, Sci. Rep. 11 (1) (2021) 10797.
[15] N. Meredith, Assessment of Implant Stability as a Prognostic Determinant, Int. J. Prosthodont. 11 (5) (1998) 491–501.
[16] F. Javed, H.B. Ahmed, R. Crespi, et al., Role of primary stability for successful osseointegration of dental implants: factors of influence and evaluation, Interv. Med. Appl. Sci. 5 (4) (2013) 162–167.
[17] N.B. Damm, M.M. Morlock, N.E Bishop, Friction coefficient and effective interference at the implant-bone interface, J. Biomech. 48 (12) (2015) 3517–3521.
[18] S. Campi, S.J. Mellon, D. Ridley, et al., Optimal interference of the tibial component of the cementless Oxford Unicompartmental Knee Replacement, Bone Joint. Res. 7 (3) (2018) 226–231.
[19] C.E. Scott, M.J. Eaton, R.W. Nutton, et al., Metal-backed versus all-polyethylene unicompartmental knee arthroplasty: proximal tibial strain in an experimentally validated finite element model, Bone Joint. Res. 6 (1) (2017) 22–30.
[20] D.M. Geraldes, U. Hansen, J. Jeffers, et al., Stability of small pegs for cementless implant fixation, J. Orthop. Res. 35 (12) (2017) 2765–2772.

[21] C.E. Post, T. Bitter, A. Briscoe, et al., A FE study on the effect of interference fit and coefficient of friction on the micromotions and interface gaps of a cementless PEEK femoral component, J. Biomech. 137 (2022) 111057.
[22] D. Janssen, R.E. Zwartelé, H.C. Doets, et al., Computational assessment of press-fit acetabular implant fixation: the effect of implant design, interference fit, bone quality, and frictional properties, P I Mech Eng H 224 (1) (2010) 67–75.
[23] T.M. Keaveny, E.F. Wachtel, C.M. Ford, et al., Differences between the tensile and compressive strengths of bovine tibial trabecular bone depend on modulus, J. Biomech. 27 (9) (1994) 1137–1146.
[24] E.F. Morgan, G.U. Unnikrisnan, A.I. Hussein, Bone mechanical properties in healthy and diseased states, Annu Rev. Biomed. Eng. 20 (2018) 119–143.
[25] M. Petrini, M. Tumedei, A. Cipollina, et al., Fixture length and primary stability: an in vitro study on polyurethane foam, Appl. Sci. 12 (5) (2022).
[26] N. Kelly, J.P. McGarry, Experimental and numerical characterisation of the elasto-plastic properties of bovine trabecular bone and a trabecular bone analogue, J. Mech. Behav. Biomed. Mater. 9 (2012) 184–197.
[27] G. Maquer, C. Mueri, A. Henderson, et al., Developing and validating a model of humeral stem primary stability, intended for in silico clinical trials, Ann. Biomed. Eng. 52 (5) (2024) 1280–1296.
[28] P.S. Patel, D.E. Shepherd, D.W Hukins, Compressive properties of commercially available polyurethane foams as mechanical models for osteoporotic human cancellous bone, BMC. Musculoskelet. Disord. 9 (2008) 137.
[29] S. Berahmani, D. Janssen, S. van Kessel, et al., An experimental study to investigate biomechanical aspects of the initial stability of press-fit implants, J. Mech. Behav. Biomed. Mater. 42 (2015) 177–185.
[30] N.E. Bishop, J.C. Hohn, S. Rothstock, et al., The influence of bone damage on press-fit mechanics, J. Biomech. 47 (6) (2014) 1472–1478.
[31] S. Rapagna, S. Berahmani, C.E. Wyers, et al., Quantification of human bone microarchitecture damage in press-fit femoral knee implantation using HR-pQCT and digital volume correlation, J. Mech. Behav. Biomed. Mater. 97 (2019) 278–287.
[32] X. Min, D. Heath, L. Marks, et al., Experimental characterisation of coefficient of friction at bone-implant interface, in: ORS 2024 Annual Meeting, Long Beach, California, 2024.
[33] ASTM F1839-01, Standard Specification for Rigid Polyurethane Foam for Use as a Standard Material For Testing Orthopaedic Devices and Instruments, American Society for Testing and Materials, Pennsylvania, 2001.
[34] J.D. Silva-Henao, R.J. Rueda Esteban, A. Marañon-Leon, et al., Post-yield mechanical properties of bovine trabecular bone – relationships with bone volume fraction and strain rate, Eng. Fract. Mech. 233 (2020).
[35] M. Ovesy, M. Aeschlimann, P.K. Zysset, Explicit finite element analysis can predict the mechanical response of conical implant press-fit in homogenized trabecular bone, J. Biomech. 107 (2020) 109844.
[36] M. Ovesy, J.D. Silva-Henao, J.W.A. Fletcher, et al., Non-linear explicit micro-FE models accurately predict axial pull-out force of cortical screws in human tibial cortical bone, J. Mech. Behav. Biomed. Mater. 126 (2022) 105002.